University of Nova Gorica
Faculty of graduate studies

Seminar

Modeling of thermomechanical phenomena during DC casting of aluminium alloys

Author: Boštjan Mavrič

Advisor: prof. Božidar Šarler

Ljubljana, May 28, 2014

Contents

1 Introduction

The DC casting is well established technology used to cast majority of aluminium intended for production of sheet ingots, extrusion billets and electrical conductors. Although the process has bee widely used for almost a century, there are still some technological problems to be understood. Due to the complex interaction between various physical phenomena, the best way to understand the technological problems is by development of advanced numerical models (Založnik, 2006; Vertnik et al., 2006).

In the seminar the main technological problems caused by the solid mechanics phenomena are presented. A new meshless approach using collocation with radial basis functions is described and some convergence properties are presented. The seminar is concluded by some preliminary results obtained with the method

2 DC Casting of Aluminium Alloys

2.1 History

Element aluminium was discovered in 1808 by H. Davy an English chemist working on electrolysis of molten salts. At its discovery aluminium was considered a precious metal with price higher than platinum or gold and was as such presented at Paris World Exhibition in 1855. Aluminium's eminent status has been permanently lost in 1888 with the discovery of Hall-Heurot process enabling mass production of aluminium.

Light, oxidation resistive metal quickly found its use in aircraft industry, especially after the discovery of an especially tough Al-Cu alloy named "duralumin". The aircraft industry growth fueled by the World War I. had increased the demand for the metal and by the 1930s all-metal aluminium planes were dominant throughout the industrialized world. Such great demand called for a technology capable of mass producing high quality aluminium ingots.

At the time, most of aluminium was cast in permanent molds weighing from 20 to 200 kg. Although this technique was usable for casting of small ingots, the quality of larger specimens was unsatisfactory. Main problems of permanent mold casting were the turbulence during the pouring leading to segregation of alloying elements, air-gap formation due to the solidification shrinkage and low cooling rate that varied across the ingot (Eskin, 2008). Several improvements of casting processes were proposed, all of them trying to remedy one of the drawbacks of permanent mold casting. The solution for most of the problems mentioned above had already been proposed for casting of steel in 1886, but failed to gain traction in mass production of aluminium. American engineer B. Atha had pouring melt in a bottomless mold and then extracting the billet from the bottom of the mold at the same rate as it solidified at the top. It was further improved by Junghaus in 1950s and is today known as continuous casting.

Although the method was revolutionary, it still had some drawbacks. The air gap still formed between the mold and the billet, and high thermal gradients caused severe inhomegenieties in structure and composition. Furthermore the casting speed remained low and the mold was hard to produce since it had to be long and have very smooth surface. The method addressing these drawbacks was developed almost simultaneously in Germany and United States in late 1930s. In this new technique the melt is poured from the top into a short, water cooled mold. The mold is closed from the bottom by a dummy block that is connected to the hydraulic lowering system. When the melt reaches a certain level, the bottom block is retracted and water cooling in form of spray or thin film is applied to the solidified shell. This detail gives the direct chill (DC) casting its name, since the ingot is cooled by direct contact between water and solidified shell, rather than by conduction trough mold walls. When the dummy block of the machine reaches the bottom of the casting pit, the process is stopped and the ingot is removed. Using empirically established recipes this technique has enabled a large variety of aluminium alloys to be cast.

Current developments in aluminium casting are being done in the direction of abandoning the mold altogether. The melt is instead held in place by an electromagnetic field that causes compressive forces to be applied to the melt. These forces also additionally stir the melt improving homogeneity of the resulting ingot. However, the start-up is difficult and the process parameters must be controlled very precisely, limiting applicability

of the technique for industrial use.

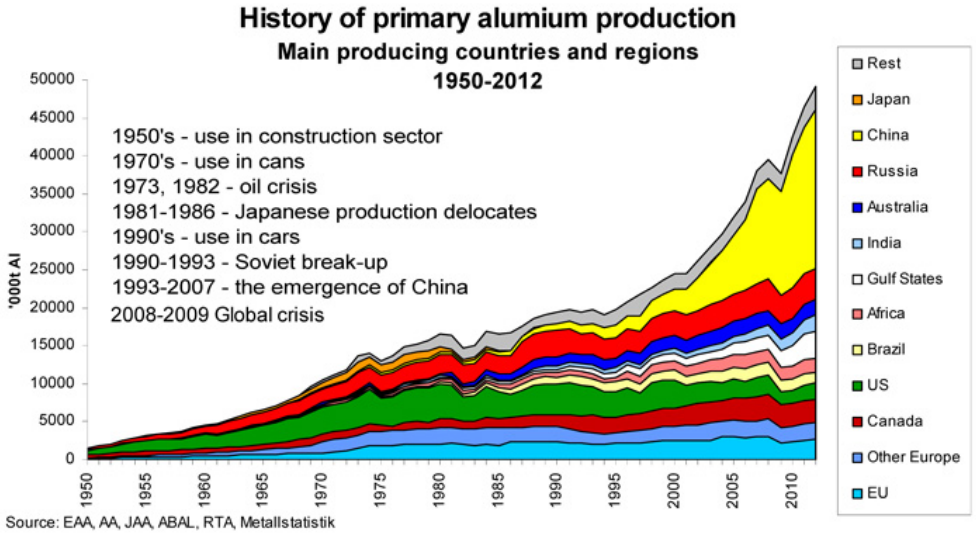

Figure 1: The history of primary aluminium production by region with explanation of events that influenced the production. (EAA, 2014)

2.2 An illustration of DC casting machine

An example of a hot-top DC casting machine is shown in Figure 2. The goal of this figure is twofold. Firstly it is supposed to give us an visual clue as to the geometrical setting of the computational problem and secondly it is to help us establish terminology used in this seminar.

The degassed melt arriving from the furnace is lead by the trenches in the casting table to a DC casting machine. The melt enters the mold from the top and starts solidifying on contact with the dummy block. When the solidified part is strong enough to support the metallostatic pressure caused by the liquid phase, the dummy block starts to retract from the mold, removing the solidified alloy. The solidified alloy takes on the role of the dummy block in the heat removal as well as in preventing the melt to escape the mold.

Since alloys do not solidify at a well defined temperature, but over a temperature range the mushy zone is formed between the solid and liquid phase. In this zone the phase transition between the states is occurring, resulting in a mixture of areas that are already solidified and areas that are still liquid. Mushy is usually thickest and the lowest at the billet center. Because of the shape it is called the sump.

The first contact of the solid phase with the mold should be on the graphite ring. This part of the casting device is used for two reasons. Firstly, the small heat conductivity of the graphite prevents the solid shell spread upward while becoming too thin to support its own weight. In case the solid shell gets too thin, it periodically collapses, which results in unwanted surface defects and introduction of oxide inclusions to the near-boundary area. Secondly, the porous structure of graphite rings allows the lubricants to be injected between the mold and the solid shell, reducing the friction and improving the overall surface quality.

As the solidified shell exits the mold, it is hit by the water spraying from nozzles mounted along the bottom circumference of the mold. The nucleate boiling that occurs

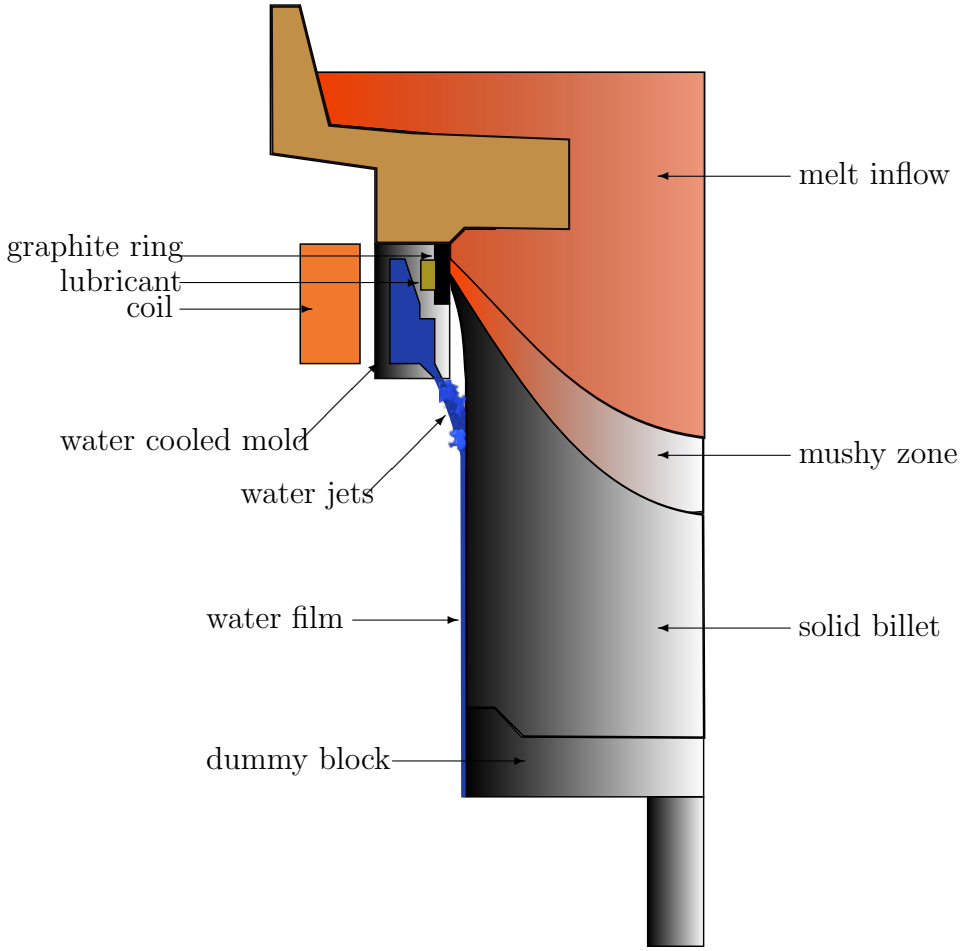

Figure 2: Illustration of an hot-top direct chill casting device.

at the contact point, provides an exceptionally efficient way to extract heat from the billet resulting in high thermal gradients near this area. The water then flows downward in form of the thin film on the surface of the billet providing additional cooling along the outer surface. In order to ensure uniform cooling, it is important to keep the water film coherent on the whole billet surface.

This entire device is inserted into a copper coil on which alternating current with frequency about 20 Hz is applied. Due to the induction in the material the outer part of the solidifying billet is subjected to the Lorentz force. The area on which the applied force is significant is limited to the regions near the billet surface due to the skin effect. If the material in this area is still in liquid state, the resulting stirring force improves the chemical structure of the cast material.

2.3 Technological problems

Although the DC casting is widely used and well established technology, there are still many aspects that can be improved with the use of numerical models. These aspects are mainly associated with the plant safety and product quality.

2.3.1 Heat transfer

The DC casting process relies on the producer's ability to sustain stationary state in the mold. A large change in heat transfer conditions can destroy the stationary state and cause the catastrophic melt bleed-out, which endangers the personnel controlling the

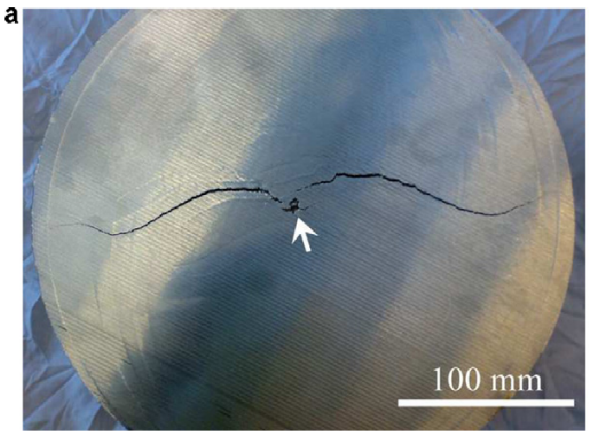

Figure 3: Hot tearing in an aluminium billet. The point where the crack initiated is marked with an arrow. (Lalpoor et al., 2011)

casting device. Two of the reasons for a change in heat transfer conditions related to the solid mechanics, are the butt curl and butt swell.

The terms are used to describe the deformation of the bottom part of the aluminium billet. The butt curl is formed because of large thermal stresses that occur when the water cooling is applied to the bottom of the billet exiting the mold. These stresses deform the billet and curve its surface away from the dummy block. The gap that forms, reduces the heat transfer trough the bottom of the block, enabling melt bleed-out. The water can also enter the gap. If the bottom is warm enough to cause vaporization on contact, the billet can start "bumping" in the dummy block.

The but swell is caused by lesser apparent solidification shrinkage of the bottom part of the billet. This bottom part is formed when the mold is closed by the dummy block. When the dummy block starts to travel downwards, the sump deepens. The liquid in the center does not provide enough resistance to prevent the thermal shrinkage of the outer solidified shell, so the shell is able to contract more than it was able to in the bottom when the center had already been solid. The bottom therefore appears to be swollen, but, in fact, the rest of the billet is more contracted. This contraction also enhances the butt curl, which can, in the worst case scenario, destabilize the billet. (Eskin, 2008)

2.3.2 Hot tearing

One of the most serious casting defects is hot tearing, the irreversible formation of a crack in the semisolid casting. The importance of hot tearing is reflected in many studies trying to understand various aspects of the phenomenon (Eskin et al., 2004; Eskin, 2008; Li, 2010; Stangeland, 2005) as well as in the development of numerical models to predict it's occurrence (Hao et al., 2010; Sistanina, 2013; Vernede, 2007).

To better understand the physical reasons for hot tearing, we should consider the solidification process of an aluminium alloy. Based on the permeability of the solid network, the process can be divided into four stages (adapted from (Eskin, 2008)).

1. *Mass feeding*, in which both, the already solidified dendrites and liquid melt are free to move.

2. *Interdendritic feeding*, in which the fluid has to flow through the already coherent solid skeleton.

3. *Interdendritic separation*, in which the liquid network becomes fragmented. With increasing solid fraction, liquid is isolated in pockets or immobilized by surface tension.

4. *Interdendritic bridging* or *solid feeding*, in which the billet has developed considerable strength and solid state creep compensates for further contraction.

Hot tearing usually occurs in the last two stages in conditions, in which the liquid feeding is not sufficient to account for the shrinkage of the material. The shrinkage can be in general divided in two parts, the solidification shrinkage and thermal shrinkage. Thermal shrinkage is well known thermal isotropic contraction, while the reason for the solidification shrinkage is the difference in densities of solid and liquid phases. The thermal shrinkage is the main factor for stress occurrence in already solidified material while the solidification shrinkage is most relevant during the third stage of the solidification, when the liquid network becomes fragmented.

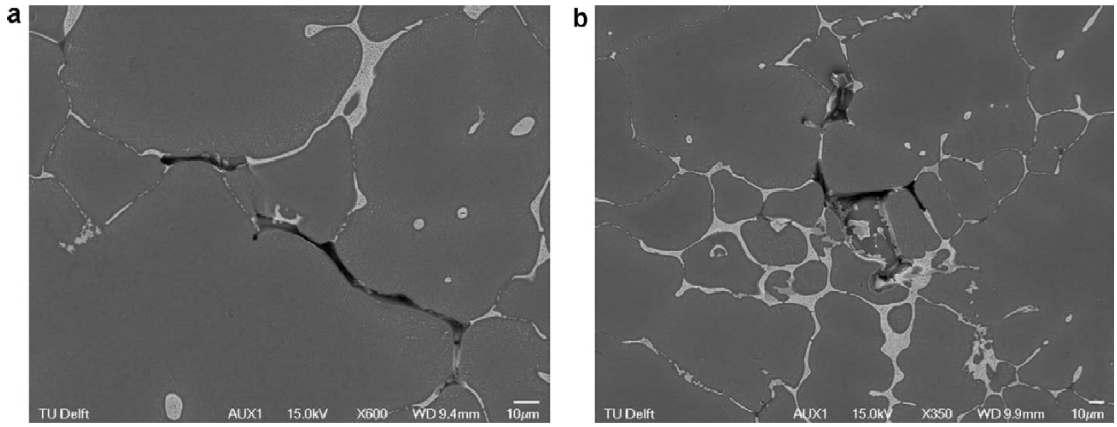

Figure 4: Image of the voids that form in the solidified metal due to the insufficent feeding. (Lalpoor et al., 2010)

As a result of the shrinkage stresses develop in the ingot. The existence of areas with tensile stress is one of the most important conditions for hot tearing. To the occurrence of hot tears also the fact, that the yield stress decreases with increasing temperature. If the tensile stresses in an area increase over this value, the dendritic bridges that have formed collapse, initiating a hot tear.

The alloy composition is also an important factor determining the hot-tearing probability. Different thermo-mechanical properties, different solidification range and variances in microstructure resulting from different chemical composition can make hot-tearing even more difficult to predict.

3 Thermomechanics

In linear solid mechanics, two quantities have a fundamental role. These are the stress and the strain tensor fields. Let us quickly refresh their definitions.

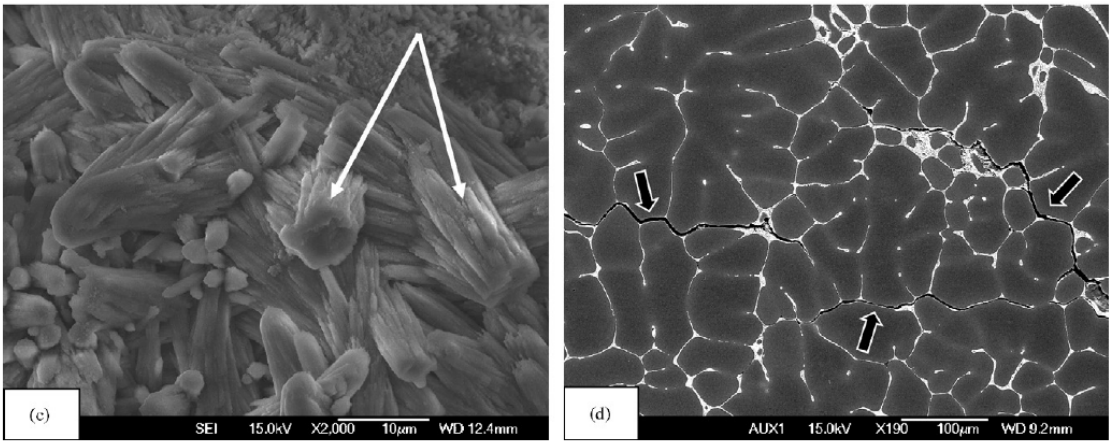

Figure 5: Image of the hot tearing crack obtained by electron microscope. In the figure (c) the failed interdendritic bridges are pointed to by the white arrows. In figure (d) some cracks caused by the stress are indicated by the black arrows. (Lalpoor et al., 2010)

The deformation of an elastic body is described by displacement vector field $\boldsymbol{u}(\boldsymbol{r})$, defined as the difference between the location of a chosen point on the deformed and non-deformed body. The displacement field is assumed to be continuous, so that derivatives are well defined. The strain tensor ε is then defined as

$$\varepsilon_{\xi\chi} = \frac{1}{2}\left(\frac{\partial u_\xi}{\partial x_\chi} + \frac{\partial u_\chi}{\partial x_\xi} - \frac{\partial u_\kappa}{\partial x_\chi}\frac{\partial u_\kappa}{\partial x_\xi}\right). \tag{1}$$

Here, and in the following chapters we make use of the Einstein's summation convention. The Greek indices denote the vector components in the Cartesian coordinates. In case of small deformations we can neglect the last term in the above expression, which results in the usual definition of the strain tensor as the symmetric part of the displacement field gradient.

To formulate the definition of stress tensor, we need to consider a closed surface S inside the elastic body. If there are stresses present in the body, then we can assume that a force $\mathrm{d}\boldsymbol{F}$ is acting on each small part $\mathrm{d}S$ of the surface. The ratio of these two quantities is called *traction* $\boldsymbol{t}$. The linear mapping, that maps the normal of the surface element $\boldsymbol{n}$ to the traction prescribed on the mentioned surface element is the stress tensor σ. It can be formally defined as

$$t_\xi = \sigma_{\xi\chi} n_\chi. \tag{2}$$

Using the same setting we can also derive the equilibrium condition. Let us firstly allow for an additional external body force to be acting on the considered body. The distribution of the force can be described with $\boldsymbol{f}(\boldsymbol{r})$. The force equilibrium for the body B with surface S is given by

$$\oint_S \boldsymbol{t}\mathrm{d}S + \int_B \boldsymbol{f}\mathrm{d}V = 0 \tag{3}$$

The definition 2 is used to express the equilibrium condition in terms of stress tensor. Using the divergence theorem, we arrive at

$$\int_B \left(\vec{\nabla}\cdot\sigma + \boldsymbol{f}\right)\mathrm{d}V = 0. \tag{4}$$

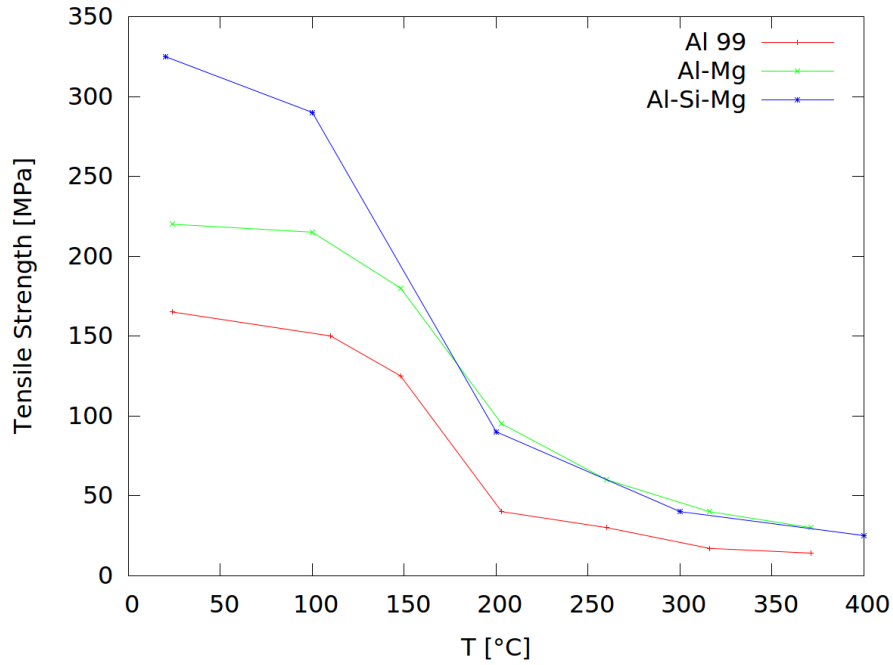

Figure 6: Tensile strength behavior for several aluminium alloys. We can see, that the tensile strength changes by an order of magnitude with varying temperature. Data adapted from (Brandes and Brook, 1999).

By reducing the volume of the interior of the surface to such extent that the integration term can be assumed constant, we see that the equilibrium condition is

$$\vec{\nabla} \cdot \sigma + \boldsymbol{f} = 0. \tag{5}$$

3.1 Linear theory

To be able to write the equilibrium condition (5) in terms of deformation vector, we need to assume an constitutive law connecting the stress and strain tensors. The most general linear law of this form is specified by a fourth order elastic tensor. In case of an isotropic body only two constants are enough to describe the tensor and the relation known as the Hooke's law is given by

$$\sigma_{\xi\chi} = \lambda \varepsilon_{\kappa\kappa} \delta_{\xi\chi} + 2G\varepsilon_{\xi\chi}. \tag{6}$$

The λ stays for Lamé parameter and G for the shear modulus. The δ symbol stands for Kronecker delta.

In order to justify the label thermo in thermomechanics it is necessary to couple the temperature field with displacement. To do this, we need to take a short detour in the thermodynamics. We introduce the strain energy function W defined by

$$\mathrm{d}W = \sigma_{\xi\chi} \mathrm{d}\varepsilon_{\xi\chi}. \tag{7}$$

It can be shown that such a function describes the internal energy of an isentropic process or the free energy of isothermal process (Fung and Tong, 2008). In case of an isotropic solid, this function can be written as

$$W = \frac{\lambda}{2} \varepsilon_{\xi\xi}^2 + G\varepsilon_{\xi\chi}\varepsilon_{\xi\chi}. \tag{8}$$

To describe the thermoelastic coupling we need to introduce additional terms in the strain energy function. The lowest order contribution is of the first order in both, strain and temperature. New strain energy function for isotropic solid has therefore the form

$$W = \frac{\lambda}{2}\varepsilon_{\xi\xi}^2 + G\varepsilon_{\xi\chi}\varepsilon_{\xi\chi} - \beta(T - T_{ref})\varepsilon_{\xi\chi}. \tag{9}$$

In this expression β is the coefficient describing thermal expansion, and T_{ref} is the reference temperature, at which we assume the thermal stresses to be zero. Using the definition of the strain energy function (7), the strain tensor definition, and the equilibrium equation (5) we obtain the equilibrium equation in terms of the displacement

$$G\nabla^2\boldsymbol{u} + (G + \lambda)\nabla\nabla\cdot\boldsymbol{u} = \nabla\left(\beta\left(T - T_{ref}\right)\right) - \boldsymbol{f} \tag{10}$$

The coefficient β is given by $\beta = \alpha E/(1-2\nu)$, where α is the coefficient of linear expansion defined in the relation

$$\varepsilon_{\xi\chi} = \delta_{\xi\chi}\alpha(T - T_{ref}). \tag{11}$$

By using this approach we manage to obtain the coupling in one direction only, namely for a given temperature field, we are able to calculate the stresses. To achieve thermodynamic consistency, we should also account for the inverse coupling. The derivation of the coupling comes from the consideration of the rate of entropy production (Fung and Tong, 2008). In order to simplify the equations we use thermodynamic quantities given per unit mass e.g. $F = \int \rho f \mathrm{d}V$. The entropy production rate is given by

$$\rho\dot{s} = \rho\frac{\partial s}{\partial\varepsilon_{\xi\chi}}\dot{\varepsilon}_{\xi\chi} + \rho\frac{\partial s}{\partial T}\dot{T} \tag{12}$$

From the thermodynamics we know the connection between the entropy production rate and the heat flux $\boldsymbol{j}$

$$\rho\dot{s} = -\frac{1}{T}\vec{\nabla}\cdot\boldsymbol{j} \tag{13}$$

and the definition of the heat capacity

$$C_v = -T\frac{\partial^2 F}{\partial T^2}. \tag{14}$$

Our aim is to rewrite the equation (12) in terms of free energy. The free energy of an isotropic elastic material is given by

$$\rho f = W - \rho T s, \tag{15}$$

where W is the strain energy function. From the free energy definition it is clear that we have $-s = \partial f/\partial T$. The equation (12) can now be written in terms of free energy and heat current

$$-\frac{1}{T}\vec{\nabla}\cdot\boldsymbol{j} = -\rho\frac{\partial f}{\partial\varepsilon_{\xi\chi}\partial T}\dot{\varepsilon}_{\xi\chi} - \rho\frac{\partial^2 f}{\partial^2 T}\dot{T} \tag{16}$$

The definitions of heat capacity and free energy can be used to replace the partial derivatives of the free energy. By employing the definition of the heat flux from Fourier's law $\boldsymbol{j} = -\lambda\vec{\nabla}T$ we get the coupling equation that we were looking for.

$$\frac{\partial}{\partial x_\xi}\left(k_{\xi\chi}\frac{\partial T}{\partial x_\chi}\right) = \rho C_v\frac{\partial T}{\partial t} + T\beta_{\xi\chi}\frac{\partial\varepsilon_{\xi\chi}}{\partial t} \tag{17}$$

One can imagine that the physical problems with the governing equations listed above are quite difficult to solve. In order to obtain results relevant in engineering, we have to introduce some approximations. The equations that we have written deal with transient problem, so the straightforward simplification is to limit ourselves on quasi-static problems, where all the fields are assumed to be stationary.

The fact that the adiabatic expansion of the gas is accompanied by a drop in its temperature is known as Joule-Kelvin phenomenon (Žumer and Kuščer, 2006). The equation describing the same phenomenon for solids can be obtained from equation (17), by forbidding the heat conduction ($\vec{\nabla} j = 0$). This gives us the equation connecting the rate of change of temperature with the strain rate.

$$\frac{\partial T}{\partial t} = -\frac{T\beta}{\rho C_v}\frac{\partial e_{\chi\chi}}{\partial t}. \tag{18}$$

The coefficient in front of the strain rate has in case of aluminium value $\approx$ 1K. To estimate the strain rate, we assume that all the boundary conditions and body forces are stationary. The only contribution to the strain rate is then the thermal expansion given by (11). The increase of temperature $\mathrm{d}T$ in time interval $\mathrm{d}t$ is then the sum of the increase due to the thermal conduction $\mathrm{d}T_{con}$ and the increase due to the strain rate $\mathrm{d}T_{\varepsilon}$. The increase of the temperature is then given by $\mathrm{d}T = (1 + \alpha 1\mathrm{K})\mathrm{d}T_{con}$. Since the value of α is approximately $10^{-5}K^{-1}$, the contribution to the temperature increase due to the strain rate is negligible.

Our problem therefore consists of two separate problems, the problem of heat conduction, which is in case of DC-casting complicated enough to deserve its own semiar, and the solid mechanics problem with terms describing the effects of the temperature expansion given by the equation (10).

4 State of the art numerical models

4.1 DC casting models

Since the results in this field are highly valued in the industry, many studies have been performed. First numerical results (Fjær and Mo, 1990; Weckman and Niessen, 1992; Drezet and Rappaz, 1995), albeit limited to two-dimensional cases, started to appear as soon as the computational power became cheap enough to make this kind of studies feasible. As the computational capabilities increased, the models started to become fully three dimensional and also accounted for transient situations in the beginning and at the end of the casting (Williams et al., 2003). The authors also started to trust the commercial computational packages (mainly using the finite element method) and the models relying on the custom codes were getting rarer. In the custom codes also mainly the finite element method is used (Kumar et al., 2012). During this development the constitutive laws used in the models closely followed the cutting-edge relations derived from experimental and theoretical studies (Ludwig et al., 2005; Dantzig and Rappaz, 2009).

Although the solutions for deformation and stress fields are valuable results by themselves, some other quantities are of greater importance for industrial applications. These quantities usually help the engineers determine the areas where certain casting defects

could occur at given casting conditions. The quantities are usually estimated by a post-processing step. The hot-tearing probability (Lalpoor et al., 2011) is estimated using one of the many hot-tearing criteria (Eskin et al., 2004), the critical crack size is estimated from the fracture theory and porosity from a criterion given by physical metallurgy (Dantzig and Rappaz, 2009).

4.2 Meshless methods

In conventional methods the mesh generation is an important step during the numerical solution. In case of the FEM and finite volume method (FVM) the domain has to be polygonized, which is an demanding and time consuming task. The finite difference method (FDM) is defined on a regular grid, which severely reduces the applicability of the method for irregular geometries.

The many variants of meshless methods try to alleviate both problems (Liu, 2010). In general the meshless methods either use the variational approach of the FEM or try to generalize the FDM method. The latter approach is the one we are interested in. The main reason is the simplicity of the implementation and applicability to many different physical phenomena.

Over the years various approaches to generalizing the FDM (Liszka and Orkisz, 1980; Shirobokov, 2006; Sadat and Prax, 1996) were proposed. These methods were able to obtain quite accurate results, but they were plagued by ill-conditioned interpolation problem for some node arrangements. To bypass this problem, the finite difference formulas were suggested to be calculated using a set of (conditionally) positive definite functions, meaning that the interpolation problem was always well defined. One such set are the radial basis functions, in particular the multiquadrics.

Multiquadrics (MQ) were first used for PDE solving in the two fundamental articles published by Kansa in 90's (Kansa, 1990a,b). In these articles, the MQs were used in spectral mode, meaning that the solution was interpolated on the whole computational domain, and not only on the small stencils as in the case of FDM. The global interpolation approach limits the number of discretization points that can be used. Since all the functions used are of the same shape, only their origin is shifted, the functions with origins close enough become linearly dependent, which causes the system of equations to become ill conditioned.

Improvements were proposed in the direction of abandoning the global interpolation and interpolating the solution only locally (Lee et al., 2003; Tolstykh and Shirobokov, 2003). This approach has turned out to be very robust, allowing for great flexibility of the method. The method has since been successfully applied to many physical problems including problems from industry (Vertnik, 2010). The only problem left is the determination of the optimal value of the shape parameter, that defines the scale of the function. Since there is no sound theory that can be used, various heuristic methods are being proposed (Rippa, 1999; Simonenko et al., 2014). Some other efforts are going in the direction of factoring out the ill-conditioning due to the inappropriate shape parameter values (Fornberg et al., 2011) or deriving extrapolating formulas that help expand the range of usable shape parameter values (Fornberg and Wright, 2004).

5 A meshless solution for thermomechanics

Firstly, we set up some notation used for the general formulation of the method. Let us have a compact domain Ω with boundary Γ. We are solving the differential equation for $\boldsymbol{u}(\boldsymbol{r})$, given by operator $\mathcal{D}(\boldsymbol{r})$

$$D_{\xi\chi}(\boldsymbol{r})u_\chi(\boldsymbol{r}) = g_\chi(\boldsymbol{r}) \tag{19}$$

with boundary conditions specified by the operator $\mathcal{B}(\boldsymbol{r})$

$$B_{\xi\chi}(\boldsymbol{r})u_\chi(\boldsymbol{r}) = b_\chi(\boldsymbol{r}). \tag{20}$$

The method being developed is a generalization of the finite difference method to irregular node arrangements. At first, the computational points, called nodes, are distributed over the interior and on the boundary of the domain, thus defining the computational domain. Let us denote the position of l-th node with $\boldsymbol{r}_l$. To generate the approximation of the solution at each node, a set of neighboring points ${}_l\Omega$, called the subdomain, needs to be chosen. Although the choice of the subdomain is in principle arbitrary, given that every subdomain overlaps with at least one of the others, usually a certain number of nearest neighbors is chosen. Let us denote the number of nearest neighbors in subdomain of the node with index l by ${}_lN$. With the choice of the subdomain, we have introduced a mapping ${}_ls$ from the set of integers from 1 to ${}_lN$ to the global index assigned to every computational node. The solution is then interpolated over the nodes in the subdomain using translations of MQ's. An MQ centered at node i is given by

$$\Phi_i(\boldsymbol{r}) = \sqrt{\sum_\xi (r - r_i)^2 + c^2}. \tag{21}$$

Since MQ's are only conditionally positively definite, the interpolation problem where only MQ's are used is not well defined (Wendland, 2004). The solution is to augment the interpolation problem with m monomials $p_i(r)$, of up to linear order. The solution approximation is then given by

$$u_\xi(\boldsymbol{r}) \approx \sum_i^{{}_lN} {}_l\alpha_{i,\xi}\Phi_i(\boldsymbol{r}) + \sum_{i={}_lN+1}^{{}_lN+m} {}_l\alpha_{i,\xi}p_i(\boldsymbol{r}) = \sum_i^{{}_lN+m} {}_l\alpha_{i,\xi}\Psi_i(\boldsymbol{r}). \tag{22}$$

The main idea of the method is to use the above approximation to estimate the differential operators of the vector field $\boldsymbol{u}(\boldsymbol{r})$. Since the coefficients ${}_l\alpha_{i,\xi}$ are constants, it is straightforwad that

$$D_{\xi\chi}(\boldsymbol{r})u_\chi(\boldsymbol{r}) \approx \sum_{i,\xi}^{{}_lN+m} {}_l\alpha_{i,\xi}\, D_{\xi\chi}(\boldsymbol{r})\Psi_i(\boldsymbol{r}). \tag{23}$$

The coefficients ${}_l\alpha_{i,\xi}$ are determined by collocation of the solution values at each domain point. For the points on the boundary the boundary condition is imposed. In this manner we obtain an interpolant that analytically satisfies the boundary conditions. The system of equations is written in matrix form

$$\sum_{i,\chi} {}_lA_{ji,\xi\chi}\, {}_l\alpha_{j,\chi} = {}_l\gamma_{j,\xi} \tag{24}$$

defining the local collocation matrix A and collocation right-hand side vector γ. The elements of the collocation matrix are given by

$$ {}_lA_{ji,\xi\chi} = \begin{cases} \Psi_i(\boldsymbol{r}_{{}_ls(j)})\delta_{\xi\chi} & \text{if} \quad \boldsymbol{r}_{{}_ls(j)} \in \Omega \\ B_{\xi\chi}(\boldsymbol{r}_{{}_ls(j)})\Psi_i(\boldsymbol{r}_{{}_ls(j)}) & \text{if} \quad \boldsymbol{r}_{{}_ls(j)} \in \Gamma \\ p_j(\boldsymbol{r}_j)\delta_{\xi\chi} & \text{if} \quad j \geq {}_lN \end{cases} \tag{25} $$

and the elements of the right-hand side vector by

$$ {}_l\gamma_{j,\xi} = \begin{cases} u(\boldsymbol{r}_{{}_ls(j)}) & \text{if} \quad \boldsymbol{r}_{{}_ls(j)} \in \Omega \\ b_\chi(\boldsymbol{r}_{{}_ls(j)}) & \text{if} \quad \boldsymbol{r}_{{}_ls(j)} \in \Gamma \\ 0 & \text{if} \quad j \geq {}_lN \end{cases} . \tag{26} $$

Now we have everything set up to discretize the differential operator $\mathcal{D}$. As it has already been noticed it is possible to use the RBF-interpolant to estimate the value of a differential operator. At each node l we can approximate the operator value by

$$ D_{\xi\chi}(\boldsymbol{r}_l)u_\chi(\boldsymbol{r}_l) \approx \sum_{i,\xi}^{{}_lN+m} {}_l\alpha_{i,\xi}\, D_{\xi\chi}(\boldsymbol{r}_l)\Psi_i(\boldsymbol{r}_l). \tag{27} $$

The system given by equation (24) can be formally solved by calculating the matrix A^{-1}. The expansion cefficients can be expressed in terms of components of vector γ. The partial differential equation component ξ at node l is then written as

$$ \sum_{k,\chi} {}_l\gamma_{k,\chi} \sum_{i,\zeta} {}_lA^{-1}_{ik,\zeta\chi} D_{\xi\zeta}\Psi_i(\boldsymbol{r}_l) = g_{l,\xi}. \tag{28} $$

The equation can be changed in to a somewhat clearer form by using the definition of the components of the vector γ. We see that the vector has two types of components. The unknown solution values and the values specified by boundary conditions. The specified values should be moved to the right-hand side, leaving only the unknowns on the left hand side. To achieve this we introduce the set indicators Υ_i^Δ which evaluate to 1, if the node with index i is in the set Δ and to zero otherwise. Using this notation the equation (28) gets the form

$$ \sum_{k,\chi} u(\boldsymbol{r}_{{}_ls(k)})_\chi \Upsilon^\Omega_{{}_ls(k)} \sum_{i,\zeta} {}_lA^{-1}_{ik,\zeta\chi} D_{\xi\zeta}\Psi_i(\boldsymbol{r}_l) = g_{l,\xi} - \sum_{k,\chi} b(\boldsymbol{r}_{{}_ls(k)})_\chi \Upsilon^\Gamma_{{}_ls(k)} \sum_{i,\zeta} {}_lA^{-1}_{ik,\zeta\chi} D_{\xi\zeta}\Psi_i(\boldsymbol{r}_l). \tag{29} $$

This equation represents the system of linear equations specifying the discretized partial differential equation 19. The matrix representing the system of equations is sparse, meaning that it can be solved efficiently by specialized solvers.

Another nice property of the method is the fact that the order of the approximation depends on the number of subdomain nodes, allowing us to increase the approximation order by increasing the number of the nodes.

5.1 Numerical example

To demonstrate the feasibility of the method, we consider a simple two-dimensional thermomechanics problem. We are solving a problem on the square $[0,1]\times[0,1]$ with Dirichlet

boundary condition at $(0, y)$, traction free condition at $(1, y)$ and Neumann boundary conditions on the two remaining sides. The domain and boundary conditions are illustrated in Figure 7. In the same figure also examples of subdomains for different number of subdomain nodes are shown. The numbers have been chosen so, that the number of free parameters in the interpoaltion system is the same as the number of terms in the Taylor series expansion up to a certain order. The number of terms up to the second order is 6, up to third order 10, up to fourth order 15 and up to fifth order 21.

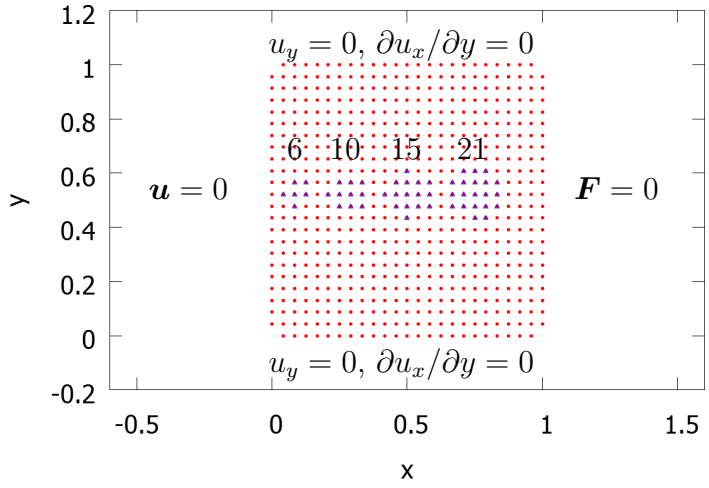

Figure 7: An example of node arrangement used to obtain the solution. The domains for different choices of the number of neighbors used for interpolation are indicated with blue squares.

The temperature field was chosen to vary as $T(\boldsymbol{r}) = \sin 2\pi x$. Only the x component of the analytic solution $\hat{\boldsymbol{u}}(\boldsymbol{r})$ is nonzero. It is given by

$$\hat{u}(\boldsymbol{r}) = -\frac{\alpha(1+\nu)}{2\pi(1-\nu)}(\cos 2\pi x - 1). \tag{30}$$

The error measure is calculated by

$$\epsilon = \sqrt{\frac{\sum_l \left(\boldsymbol{u}(\boldsymbol{r}_l) - \hat{\boldsymbol{u}}(\boldsymbol{r}_l)\right)^2}{\sum_l \hat{\boldsymbol{u}}(\boldsymbol{r}_l)^2}}. \tag{31}$$

The dependence of the error on the number of nodes is shown in figure 8. We can see that the convergence is of the second order for subdomains with 6 and 10 nodes and of the fourth order for subdomains with 15 and 20 nodes. The errors of the two larger subdomain node counts are an order of magnitude larger.

The performance of the method depends on the value of parameter c. It is well known that the flatter the RBF are, the better the approximation is (Fornberg and Wright, 2004). On the other hand, with increasing the shape parameter the condition number of matrix A also increases. We therefore expect an optimal shape parameter to exist. The dependence of the shape parameter on the error is shown in Figure 9. As we have expected we can see that for all the subdomain node counts there exists an optimal value, which gets smaller with increasing the subdomain node count count.

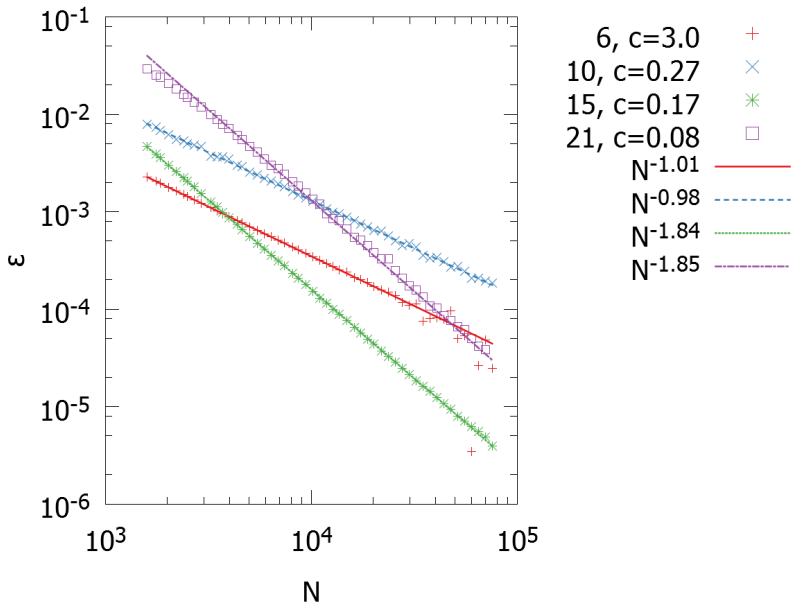

Figure 8: The convergence rates for different numbers of nodes in the subdomain.

That the reason for the error increase at large shape parameters truly is the condition number of the collocation matrix can be shown by comparing the value of the condition number with method error. This comparison is shown on the Figure 10. The error of the method for different values of the shape parameter and different numbers of discretization points is shown with the isoline at the collocation matrix condition number 10^{16}. We see that the method starts to perform worse as the shape parameter and number of discretization point pass above the curve. It is an interesting conclusion that the method behaves the best when the condition number is just small enough to allow the solution of the system of linear equations.

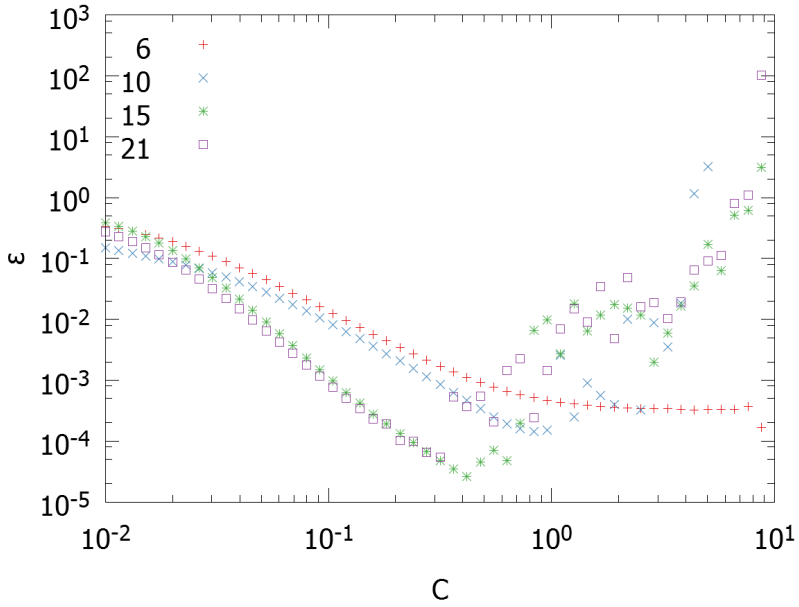

Figure 9: Error dependence on the value of the shape parameter. The existence of the optimal value is evident from the dependencies shown.

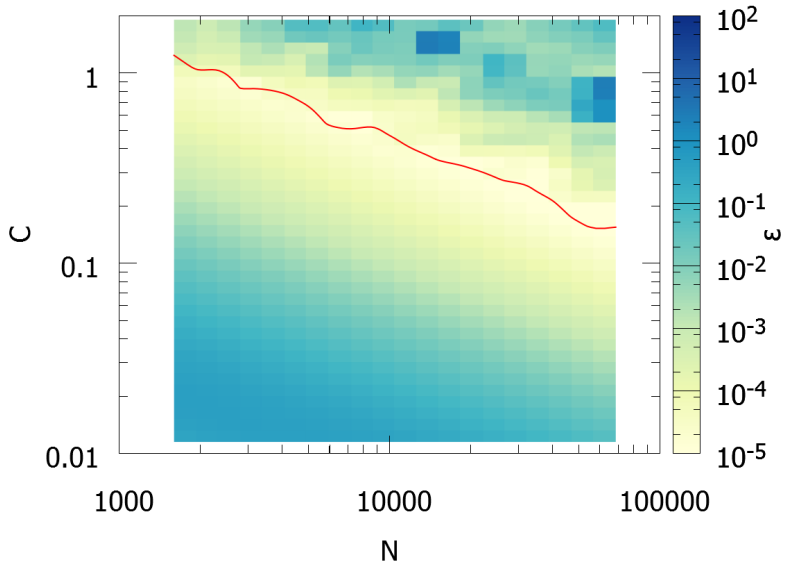

Figure 10: Error dependence on the value of the shape parameter and the number of nodes used for discretization. We can see that the method performs best when the conditioning of the interpolation problem is the worst.

5.2 DC casting model

By using elastic approximation we have already obtained some results for the industrially relevant setting. The temperature field, that is used as an input for stress calculations is calculated using other, already establised models for heat transfer and fluid flow developed in our group (Košnik et al., 2014). The material properties of course depend on the

temperature. The dependence is calculated using commercial software JMatPro. To take into account the inhomogenous material properties, we have to somewhat change the governing equation (10). In the equilibrium condition (5) we have to apply the divergence operator to the stress tensor. This operator also acts on the material constants λ and G that are used in Hooke's law resulting in some additional terms entering the governing equation. Applying the divergence operator to Hooke's law in case of an inhomogenous material we have

$$G\nabla^2\boldsymbol{u} + (G+\lambda)\nabla\nabla\cdot\boldsymbol{u} + \nabla\lambda\nabla\cdot\boldsymbol{u} + \nabla G\left(\nabla\boldsymbol{u} + (\nabla\boldsymbol{u})^T\right) = \nabla\left(\beta\left(T - T_{ref}\right)\right) - \boldsymbol{f}. \quad (32)$$

The boundary conditions are as follows: on the bottom, the deformation in z direction is set to 0, and the billet is free to move radially, outer and top surfaces are set to be traction free, and in the center the symmetry boundary condition is applied.

The results obtained for the temperature field calculated in (Košnik et al., 2014) and diplayed in Figure 11 are shown in Figure 12. The stresses are represented by colors on the deformed billet. The definitions of the stresses are given in table 1. We can see that on the top, the outer surface of the billet buckles under the weight ob the liquid in the interior, resulting in large stresses in the buckled area.

Name	Symbol	Formula
Radial stress	σ_{rr}	$(\lambda+2G)\frac{\partial u_r}{\partial r} + \lambda\left(\frac{u_r}{r} + \frac{\partial u_z}{\partial z}\right) - \beta T$
Vertical stress	σ_{zz}	$(\lambda+2G)\frac{\partial u_z}{\partial z} + \lambda\left(\frac{u_r}{r} + \frac{\partial u_r}{\partial r}\right) - \beta T$
Hoop stress	$\sigma_{\theta\theta}$	$\lambda\left(\frac{u_r}{r} + \frac{\partial u_r}{\partial r} + \frac{\partial u_z}{\partial z}\right) - \beta T$

Table 1: Table of the stress definitions.

We see that the stresses obtained from linear model are an order of magnitude larger then the typical yield stress for aluminium (Figure 6). The model is therefore not good enough and will be in future work replaced by a model capable of modeling plastic deformations.

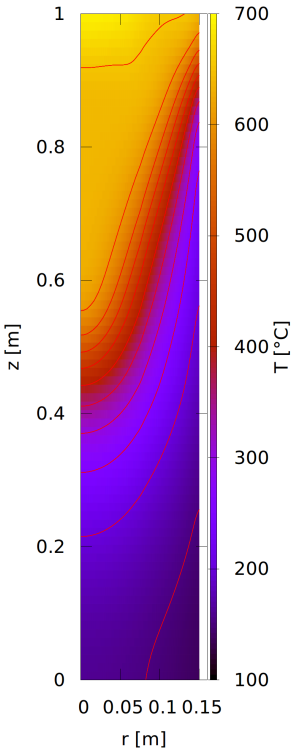

Figure 11: Temperature profile of undeformed billet obtained from the EM DC casting model described in (Košnik et al., 2014). The isolines are 50°C apart.

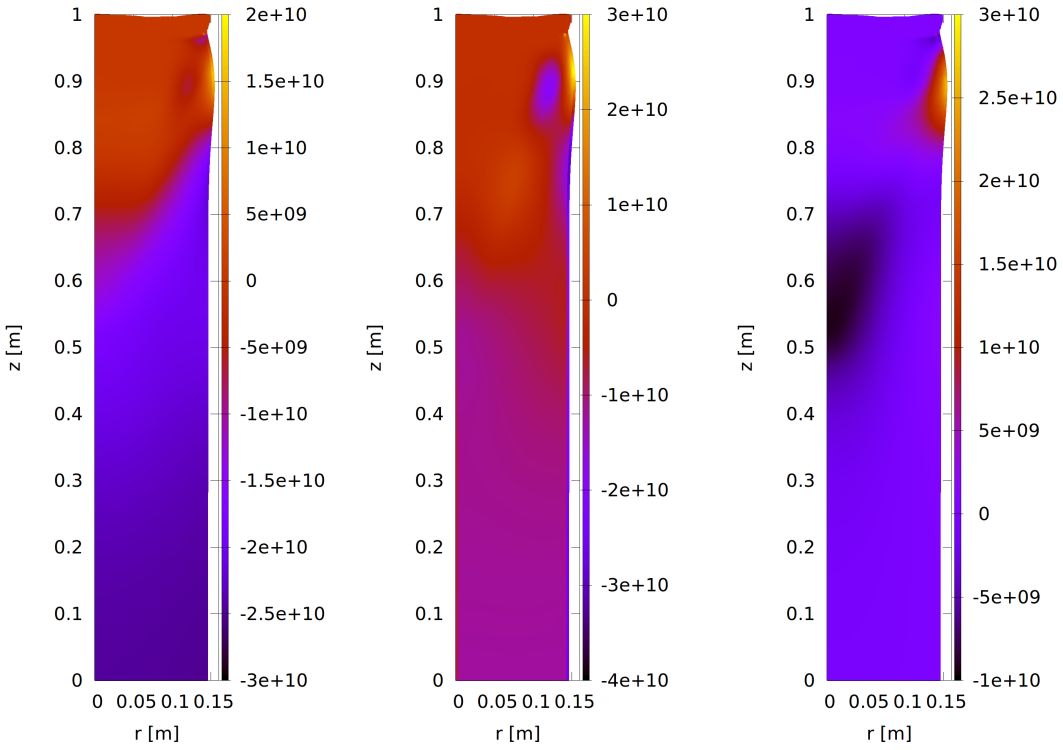

(a) Radial stress [Pa] (b) Vertical stress [Pa] (c) Hoop stress [Pa]

Figure 12: Stresses and deformations during DC casting obtained from elastic model.

6 Conclusion

Local radial basis function collocation method is a suitable tool for modeling of solid mechanics phenomena during DC casting. The accuracy of the method can be varied by changing the number of subdomain points, but there exists a limit on the accuracy which is a consequence of ill-conditioned collocation problem. Despite the accuracy limit, the method is accurate enough to enable us to obtain solutions for industrially relevant problems. As we have seen the model has to be improved in order to account for plastic phenomena. The development of such a model would help expanding the knowledge about the DC casting, which would result in improving the yield of the casting process and the quality of products.

7 Bibliography

References

Brandes, E. A. and Brook, G. B., editors (1999). *Smithells Metals Reference Book*. Butterworth Heinemann, 7 edition.

Dantzig, J. and Rappaz, M. (2009). *Solidification*. Engineering sciences. EFPL Press.

Drezet, J. M. and Rappaz, M. (1995). Thermomechanical effects during direct chill and electromagnetic casting of aluminum alloys Part II: Numerical simulation. In Evans, J., editor, *Light Metals*, pages 941–950. The Minerals, Metals & Materials Society.

EAA (2014). European Aluminium Asociation webpage, obtained on 19/5/2014. http://www.alueurope.eu/production-primary-aluminium-production-evolution-worldwide/.

Eskin, D. (2008). *Physical Metallurgy of Direct Chill Casting of Aluminum Alloys*. Advances in Metallic Alloys. Taylor & Francis.

Eskin, D., Suyitno, and Katgerman, L. (2004). Mechanical properties in the semi-solid state and hot tearing of aluminium alloys. *Progress in Materials Science*, 49(5):629–711.

Fjær, H. G. and Mo, A. (1990). ALSPEN-A mathematical model for thermal stresses in direct chill casting of aluminum billets. *Metallurgical Transactions B*, 21(6):1049–1061.

Fornberg, B., Larsson, E., and Flyer, N. (2011). Stable computations with Gaussian radial basis functions. *SIAM Journal on Scientific Computing*, 33(2):869–892.

Fornberg, B. and Wright, G. (2004). Stable computation of multiquadric interpolants for all values of the shape parameter. *Comput. Math. Appl.*, 48:853–867.

Fung, Y. C. and Tong, P. (2008). *Classical and Computational Solid Mechanics*, volume 1 of *Advanced Series in Engineering Science*. World Scientific.

Hao, H., Maijer, D., Wells, M., Phillion, A., and Cockcroft, S. (2010). Modeling the stress-strain behavior and hot tearing during direct chill casting of an AZ31 magnesium billet. *Metallurgical and Materials Transactions A*, 41(8):2067–2077.

Kansa, E. (1990a). Multiquadrics—A scattered data approximation scheme with applications to computational fluid-dynamics—I surface approximations and partial derivative estimates. *Computers & Mathematics with Applications*, 19(8–9):127–145.

Kansa, E. (1990b). Multiquadrics—A scattered data approximation scheme with applications to computational fluid-dynamics—II solutions to parabolic, hyperbolic and elliptic partial differential equations. *Computers & Mathematics with Applications*, 19(8–9):147–161.

Košnik, N., Vertnik, R., and Šarler, B. (2014). Simulation of low frequency electromagnetic DC casting. *Materials Science Forum*, 790-791:390–395.

Kumar, P. P., Nallathambi, A. K., Specht, E., and Bertram, A. (2012). Mechanical behavior of mushy zone in DC casting using a viscoplastic material model. *Technische Mechanik*, 32:342–357.

Lalpoor, M., Eskin, D., Ruvalcaba, D., Fjær, H., Cate, A. T., Ontijt, N., and Katgerman, L. (2011). Cold cracking in DC-cast high strength aluminum alloy ingots: An intrinsic problem intensified by casting process parameters. *Materials Science and Engineering: A*, 528(6):2831–2842.

Lalpoor, M., Eskin, D., ten Brink, G., and Katgerman, L. (2010). Microstructural features of intergranular brittle fracture and cold cracking in high strength aluminum alloys. *Materials Science and Engineering: A*, 527(7–8):1828–1834.

Lee, C. K., Liu, X., and Fan, S. C. (2003). Local multiquadric approximation for solving boundary value problems. *Computational Mechanics*, 30(5-6):396–409.

Li, S. (2010). *Hot Tearing in Cast Aluminum Alloys: Measures and Effects of Process Variables* . PhD thesis, Worcester Polytechnic Institute.

Liszka, T. and Orkisz, J. (1980). The finite difference method at arbitrary irregular grids and its application in applied mechanics. *Computers & Structures*, 11(1–2):83–95. Special Issue-Computational Methods in Nonlinear Mechanics.

Liu, G. (2010). *Mesh Free Methods: Moving Beyond the Finite Element Method*. Taylor & Francis.

Ludwig, O., Drezet, J.-M., Martin, C., and Suéry, M. (2005). Rheological behavior of Al-Cu alloys during solidification constitutive modeling, experimental identification, and numerical study. *Metallurgical and Materials Transactions A*, 36(6):1525–1535.

Rippa, S. (1999). An algorithm for selecting a good value for the parameter c in radial basis function interpolation. *Advances in Computational Mathematics*, 11(2-3):193–210.

Sadat, H. and Prax, C. (1996). Application of the diffuse approximation for solving fluid flow and heat transfer problems. *International Journal of Heat and Mass Transfer*, 39(1):214–218.

Shirobokov, D. (2006). On the construction of second-to-fourth-order accurate approximations of spatial derivatives on an arbitrary set of points. *Computational Mathematics and Mathematical Physics*, 46(6):1023–1043.

Simonenko, S., Bayona, V., and Kindelan, M. (2014). Optimal shape parameter for the solution of elastostatic problems with the RBF method. *Journal of Engineering Mathematics*, 85(1):115–129.

Sistanina, M. (2013). *Prediction of Hot Tearing Formation in Metallic Alloys Using a Granular Approach* . PhD thesis, EPFL.

Stangeland, A. (2005). *Development of Thermal Strain during Solidification of Aluminium Alloys* . PhD thesis, University of Oslo.

Tolstykh, A. I. and Shirobokov, D. A. (2003). On using radial basis functions in a "finite difference mode" with applications to elasticity problems. *Computational Mechanics*, 33(1):68–79.

Vernede, S. (2007). *A Granular Model of Solidification as Applied to Hot Tearing*. PhD thesis, EPFL.

Vertnik, R. (2010). *Heat and Fluid Flow Simulation of the Continuous Casting of Steel by a Meshless Method*. PhD thesis, University of Nova Gorica.

Vertnik, R., Založnik, M., and Šarler, B. (2006). Solution of transient direct-chill aluminium billet casting problem with simultaneous material and interphase moving boundaries by a meshless method. *Engineering Analysis with Boundary Elements*, 30(10):847–855.

Žumer, S. and Kuščer, I. (2006). *Toplota*. DMFA.

Weckman, D. and Niessen, P. (1992). A numerical simulation of the D.C. continuous casting process including nucleate boiling heat transfer. *Journal of Electronic Materials*, 21(1):593–602.

Wendland, H. (2004). *Scattered Data Approximation*. Cambridge Monographs on Applied and Computational Mathematics. Cambridge University Press.

Williams, A., Croft, T., and Cross, M. (2003). Modeling of ingot development during the start-up phase of direct chill casting. *Metallurgical and Materials Transactions B*, 34(5):727–734.

Založnik, M. (2006). *Modeling of Macrosegregation in Direct Chill Casting* . PhD thesis, University of Nova Gorica.